

# 1 **Ultrasensitive electrochemical determination of the cancer biomarker**

## 2 **sPD-L1 protein based on BMS-8 modified gold electrode**

3  
4 Paweł Niedziałkowski<sup>a\*</sup>, Magdalena Bojko<sup>b</sup>, Jacek Ryl<sup>c</sup>, Anna Wcisło<sup>a</sup>, Marta Spodzieja<sup>b</sup>,  
5 Katarzyna Magiera-Mularz<sup>d</sup>, Katarzyna Guzik<sup>d</sup>, Grzegorz Dubin<sup>ef</sup>, Tadeusz A. Holak<sup>d</sup>,  
6 Tadeusz Ossowski<sup>a</sup>, Sylwia Rodziewicz-Motowidło<sup>b</sup>

7  
8 <sup>a</sup>Department of Analytical Chemistry, Faculty of Chemistry, University of Gdansk,  
9 Wita Stwosza 63, 80-308 Gdansk, Poland

10 <sup>b</sup>Department of Biomedical Chemistry, Faculty of Chemistry, University of Gdansk,  
11 Wita Stwosza 63, 80-308 Gdansk, Poland

12 <sup>c</sup>Department of Electrochemistry, Corrosion and Materials Engineering, Faculty of Chemistry,  
13 Gdansk University of Technology, Narutowicza 11/12, Gdansk, 80-233, Poland

14 <sup>d</sup>Faculty of Chemistry, Jagiellonian University, Gronostajowa 2, 30-387 Krakow, Poland

15 <sup>e</sup>Malopolska Centre of Biotechnology, Jagiellonian University, Gronostajowa 7A, 30-387  
16 Krakow, Poland;

17 <sup>f</sup>Faculty of Biochemistry, Biophysics and Biotechnology, Jagiellonian University,  
18 Gronostajowa 7, 30-387 Krakow, Poland

19  
20 \*Corresponding authors, e-mail:

21 [pawel.niedzialkowski@ug.edu.pl](mailto:pawel.niedzialkowski@ug.edu.pl)

26 **Abstract**

27

28 Soluble form of Programmed Death - Ligand 1 (sPD-L1) is one of the immune  
29 checkpoint proteins which can be detected in the sera of patients with many types of cancer.  
30 Taking advantage of the BMS-8 compound properties to create a strong complex with PD-L1  
31 protein, we established a novel biosensing interface detecting sPD-L1. This work describes  
32 the chemical modification of gold electrode with BMS-8 compound which interacts with PD-  
33 L1 protein. The results show that we can confirm the presence of the sPD-L1 protein in the  
34 concentration range of  $10^{-18}$  to  $10^{-8}$  M using electrochemical impedance spectroscopy (EIS)  
35 with a limit detection (LOD) of  $1.87 \times 10^{-14}$  M for PD-L1 (S/N=3.3) and at the concentration  
36 of  $10^{-14}$  M by cyclic voltammetry (CV).

37 Additionally, the high-resolution X-ray photoelectron spectroscopy (XPS), contact  
38 angle, and surface free energy measurements were applied to confirm the successful  
39 functionalization of electrode. Moreover, we investigated the selectivity of the obtained  
40 electrode for other proteins, Programmed Death - 1 (PD-1), Cluster of Differentiation 160  
41 (CD160), and the B- and T-Lymphocyte Attenuator (BTLA) in a concentration of  $10^{-8}$  M.

42 Differentiation between of PD-L1 and PD-1 was achieved on the basis of study of  
43 frequency dispersion of capacitance effect at the surface of the modified Au electrode with  
44 BMS-8 after incubation in at various concentrations of PD-L1 and PD-1 protein in the range  
45 of  $10^{-18}$  to  $10^{-8}$  M. The significant differences are observed in the heterogeneity of PD-L1 and  
46 PD-1 measured at the same concentrations of both proteins. The results of quasi-capacitance  
47 studies demonstrate that BMS-8 strongly and specifically interacts with PD-L1 protein.

48

49

50 **Keywords:** cysteamine, sPD-L1 protein, gold electrode modification, cyclic voltammetry  
51 (CV), Electrochemical Impedance Spectroscopy (EIS).

## 52 **1. Introduction**

53

54 Every year the number of cancer cases is increasing and only in 2018, 18 million new  
55 cases were diagnosed [1]. The cancer treatments are more effective if applied in the early  
56 stages of the disease. In tumor diagnosis, many different methods are used, i.e. imaging tests,  
57 genetic testing, and measurements of tumor biomarkers [2]. The last of them is the simplest  
58 and the least invasive. The early stage of cancer is often correlated with low levels of  
59 molecular biomarkers which are difficult to detect. The series of cancer-related biomarkers  
60 are used for early diagnosis and are connected with specific cancer, e.g. carbohydrate antigen  
61 125, prostate-specific antigen, alpha fetoprotein, carbohydrate antigen 15-3, carbohydrate  
62 antigen 19-9, carcinoembryonic antigen [3–5].

63 Programmed death - ligand 1 (PD-L1) protein and its receptor, programmed death - 1  
64 (PD-1), are transmembrane, immune checkpoint proteins responsible for the negative  
65 regulation of the immune system. PD-L1 also occurs in the soluble form secreted into the  
66 serum (sPD-L1) by monocytes, macrophages, and DC [6,7] and is often overexpressed by  
67 tumor cells. Moreover, larger amount of soluble form of PD-L1 protein is detected in the sera  
68 of patients with malignant melanoma [7], renal carcinoma, nasal natural killer/T-cell  
69 lymphoma [8,9], diffuse large B-cell lymphoma [10], myeloma [11], and hepatocellular  
70 carcinoma [10]. High level of sPD-L1 impacts overall survival and is associated with the  
71 increased mortality in cancer patients [6,9,12]. It is reported that tumor-secreted sPD-L1 is  
72 biologically active and able to deliver immunosuppressive signals to lymphocyte T sPD-L1  
73 may be a potential biomarker for anti-PD-1/anti-PD-L1 therapy [7,13].

74 Currently, the diagnostic tests for PD-L1 which were approved by the Food and Drug  
75 Administration rely on immunohistochemistry (IHC). PD-L1 expressed in the tumor tissue is  
76 detected by antibodies. IHC-based tests have multiple complicating factors. Among other,

77 different IHC tests use a variation of anti-PD-L1 antibodies with diverse percentage ratio cut-  
78 off of the PD-L1 expression level for each test [14,15]. PD-L1 expression is heterogeneous in  
79 the tumor tissue and the binding sites for antibodies are limited, what combined with the  
80 analysis of biopsies specimens embedded in parafilm (FFPE) provides poorly conclusive  
81 results. IHC-approved tests cannot be compared one to another and require standardization  
82 and validation [16–18]. Additionally, enzyme-linked immunosorbent assays (ELISA) using  
83 sPD-L1 are developed but as in case of IHC test they have different detection range and apply  
84 different types of antibodies to detect sPD-L1 protein [19–27]. The comparison of different  
85 ELISA tests used for sPD-L1 detection is presented in table S1 in Supporting Information file.  
86 This situation provides a burning need to develop reliable diagnostic tests for PD-L1 protein  
87 detection what was the aim of our studies.

88 In the presented study, we developed the electrochemical biosensor for the detection of  
89 sPD-L1 protein and we performed a series of experiments confirming its effectiveness and  
90 sensitivity. BMS-8 (Bistol-Myers Sqibb – compound 8; 1-[[3-bromo-4-[(2-methyl [1,1'-  
91 biphenyl]-3-yl)methoxy]phenyl]methyl]-2-piperidinecarboxylic acid) molecule was used as a  
92 ligand covering surface of gold electrodes [23,24]. The interaction between BMS-8 and PD-  
93 L1 was confirmed by co-crystal structure (PDB: 5J8O) and thoroughly tested using Structure-  
94 activity relationship by nuclear magnetic resonance spectroscopy (SAR-by-NMR) approach  
95 while NMR excluded BMS-8 interaction with PD-1 [28]. The electrochemical studies using  
96 gold electrodes modified with BMS-8 enabled the detection of PD-L1 protein at various  
97 concentrations in the range of  $10^{-18}$  to  $10^{-8}$  M by EIS technique and at the concentration of  
98  $10^{-14}$  M by CV. We used the high-resolution X-ray photoelectron spectroscopy (XPS) to  
99 confirm the modification of gold electrodes. The electrodes were also characterized by the  
100 contact angle and surface free energy (SFE) measurements. The selectivity of presented test



- 101 towards other immune checkpoint proteins: PD-1, cluster of differentiation 160 (CD160), and
- 102 the B- and T-lymphocyte attenuator (BTLA) has been also investigated.

## 103 2. Materials and methods

104

### 105 2.1. Chemicals and reagents

106 All solvents and reagents were used without further purification. 0.1 M phosphate  
107 buffer solution (PBS), pH 7.0 was obtained according to the procedure described in [29]. 0.01  
108 M of PBS was prepared from tablets purchased from Sigma-Aldrich, dissolved in ultrapure  
109 water, and adjusted to pH 7.0 using 0.1 M hydrochloric acid and pH electrode. N-  
110 hydroxysuccinimide (NHS), 1-Ethyl-3-(3-dimethylaminopropyl)carbodiimide (EDC),  
111 cysteamine, bovine serum albumin (BSA) were purchased from Sigma-Aldrich. Ethanol,  
112 dimethyl sulfoxide (DMSO), potassium ferricyanide  $K_3[Fe(CN)_6]$ , potassium ferrocyanide  
113  $K_4[Fe(CN)_6]$  were purchased from POCh (Poland). The BMS-8 was synthesized as described  
114 previously [24,30].

115 PD-1 and PD-L1 proteins were expressed and purified as described previously [30].  
116 The recombinant human BTLA and CD160 proteins were purchased from Novoprotein, USA  
117 (company product code: C563) and ACROBiosystems, USA (company product code: BY5-  
118 H5229), respectively.

119

### 120 2.2. EIS and CV measurements

121 All electrochemical measurements were performed on MultiAutolab M204  
122 potentiostat (Metrohm, Netherlands) using three electrode system. The modified gold  
123 electrodes (1.6 mm diameter) were used as working electrodes, Ag/AgCl (0.1 M NaCl) was  
124 used as a reference electrode, and platinum wire was used as an auxiliary electrode.

125 The cyclic voltammetry measurements were conducted in the solution consisting of  
126 the equimolar amounts of 1 mM  $K_3[Fe(CN)_6]$  and  $K_4[Fe(CN)_6]$  dissolved in 0.1 M PBS, pH  
127 7.0. Before each measurement, the solution was purged with nitrogen to remove oxygen. All

128 cyclic voltammograms were recorded in the potential range of - 0.6 V to 0.8 V with the scan  
129 rate of 100 mV/s.

130 The electrochemical impedance spectroscopy analyses were performed to evaluate  
131 BMS-8/Au sensor efficiency and selectivity. All measurements were performed at room  
132 temperature in the same conditions and solutions as in CV measurements using Nova 1.1  
133 software. The analysis was carried out using Frequency Response Analyzer (FRA)  
134 implemented in MultiAutolab M204 potentiostat. The measurements were carried out in the  
135 potentiostatic mode at formal potential. The perturbation amplitude was 10 mV. The studied  
136 frequency range was set between 10 kHz and 0.1 Hz in the descending order. The EIS data  
137 were analyzed using dedicated software with NelderMead algorithm developed in LabView  
138 environment [31].

139

### 140 *2.3. X-Ray Photoelectron Spectroscopy (XPS) measurements*

141 X-Ray Photoelectron Spectroscopy (XPS) analysis was carried out using Escalab  
142 250Xi spectroscope (ThermoFisher Scientific, United Kingdom). The spectroscope was  
143 equipped with Al K $\alpha$  monochromatic X-Ray source, 250  $\mu$ m spot diameter. The applied pass  
144 energy was 15 eV. Charge compensation was controlled through low-energy Ar<sup>+</sup> ions  
145 emission by means of a flood gun, with the final calibration made with reference to the gold  
146 substrate (BE +84.0 eV) [32]. Deconvolution procedure was performed using Avantage  
147 software provided by the manufacturer. XPS analysis were performed using gold on glass  
148 substrates (11 mm  $\times$  11 mm) (Arrandee, Werther, Germany) modified in the same way as  
149 electrodes for electrochemical measurements.

150

### 151 *2.4. Contact angle and surface free energy (SFE) measurements*





152 The contact angle and surface free energy were measured using Drop Shape Analyzer  
153 — DSA100 by Krüss. The contact angles of drops of four different liquids (water, formamide,  
154 glycerol, and diiodomethane) were measured to determine the surface free energy. The image  
155 of a 4  $\mu\text{L}$  drop of the probe liquid deposited using a syringe was captured by a CCD camera  
156 connected to a graphics card. The measurements were repeated 20 times. After the digital  
157 image analysis, the average contact angle was deduced using the Young-Laplace method from  
158 the angles measured at both sides of the drop in equilibrium. The total surface free energy  $\gamma_s$   
159 and its dispersive  $\gamma_d$  and polar  $\gamma_p$  components of the surfaces were determined by the Owens,  
160 Wendt, Rabel, and Kaelble (OWRK) method from the contact angles of the four liquid drops.  
161 In addition, the polar components were expressed as their acid  $\gamma^+$  and basic  $\gamma^-$  components by  
162 the van Oss and Good method;  $\gamma^+$  and  $\gamma^-$  reflect the donor and acceptor characters  
163 of the surface [33–36].

#### 164 *2.5. Modification of bare Au electrode by cysteamine and BMS-8*

165 The bare gold electrodes before each modification by cysteamine were polished with  
166 1  $\mu\text{m}$  and then with 0.05  $\mu\text{m}$  alumina slurry. Afterward, the electrodes were rinsed twice with  
167 distilled water and then with 0.01 M PBS, pH 7.0, and dried in a stream of nitrogen. All  
168 electrodes before modification were electrochemically tested by CV and EIS measurements.

169 In the first step of modification, the electrodes were covered by formation of  
170 self-assembled monolayer (SAM) of cysteamine at the electrode surface. The gold electrodes  
171 were immersed in 5 mL of 0.018 M cysteamine solution dissolved in 99.8 % of ethanol for  
172 12 h at 4  $^\circ\text{C}$ . Subsequently, the gold electrodes were thoroughly rinsed with ethanol, then by  
173 0.01 M PBS, pH 7.0, and water to remove the residual amount of cysteamine. Subsequently,  
174 the electrodes after drying in the stream of nitrogen were used for the modification with  
175 BMS-8.



176 The procedure for the modification of the gold electrodes with BMS-8 consisted of  
177 two steps. In the first step BMS-8 was dissolved in 2 mL of DMSO to obtain 5 mM solution.  
178 The obtained solution was then added to the 2 mL vessel of the previously prepared mixture  
179 of 0.1 M of EDC, 0.05 M of NHS and 100  $\mu$ M of trimethylamine in DMSO. Secondly, after 1  
180 h the gold electrodes previously modified with cysteamine were placed in the  
181 EDC/NHS/BMS-8 mixture for 16 h at room temperature. Described procedure of BMS-8  
182 immobilization is characterized by very high reproducibility on gold electrodes as well as on  
183 various gold substrates.

184

#### 185 *2.6. Preparation of the modified Au electrodes for the electrochemical detection of PD-L1* 186 *protein*

187 The modified gold electrodes after incubation in BMS-8 solution were rinsed  
188 thoroughly with 0.01 M PBS, pH 7.0 and deionized water. Then, the electrodes were dried in  
189 a stream of nitrogen. In order to investigate the influence of blocking the nonspecific binding  
190 sites occurring on the surface we tested two approaches, the electrodes were incubated in  
191 10  $\mu$ L of 1 % BSA solution in 0.01 M PBS, pH 7.0, for 30 min and the step of incubation in 1  
192 % BSA was omitted. In the case of measurements without using BSA electrode were  
193 incubated in solution containing 2 mM 1-hexanethiol for 30 min. Then, the electrodes were  
194 incubated in various concentrations of PD-L1 protein - in  $10^{-18}$  to  $10^{-8}$  M concentration range  
195 and in  $10^{-14}$  M in the case of EIS and CV measurements, respectively. The deposition process  
196 was performed by dropping 10  $\mu$ L of protein in 0.01 M PBS, pH 7.0 onto the electrode  
197 surface and incubation for 1 h. Modified electrodes were rinsed with deionized water and 0.01  
198 M PBS, pH 7.0 before each measurement. Additionally, the test of influence of 0.01 M PBS,  
199 pH 7.0 (incubation for 1h) on the electrode was performed.



### 200 3. Results and discussion

201

#### 202 3.1. Preparation of the electrode sensitive towards PD-L1 protein

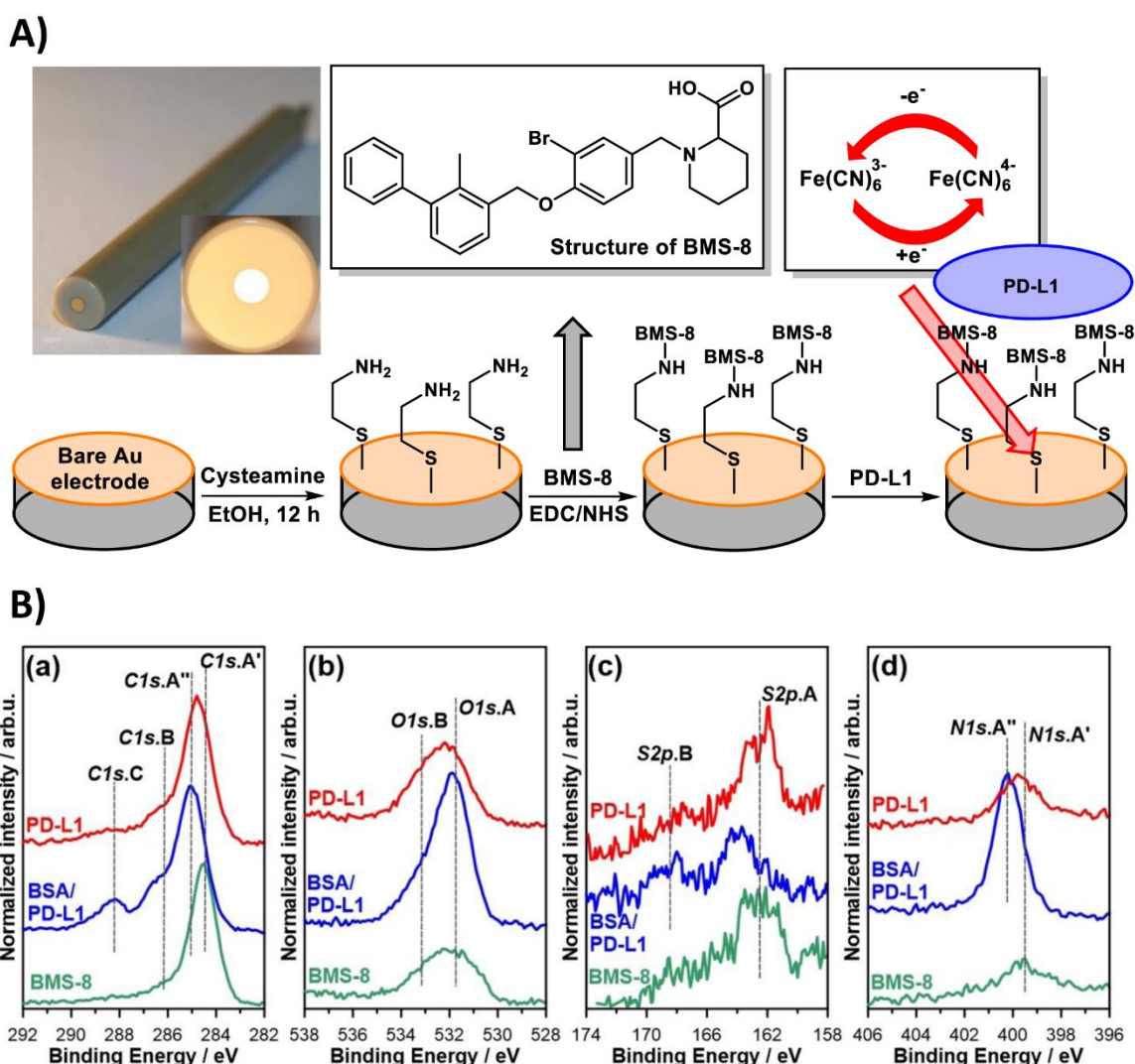
203 The detection of PD-L1 protein was conducted by anchoring of BMS-8 onto the gold  
204 electrode surface, previously modified with cysteamine. The modification procedure of the  
205 first monomolecular layer used in this work was described previously [37]. This procedure  
206 was modified by change of the solvent from water to ethanol. The modification of the gold  
207 electrodes was performed in 18 mM solution of cysteamine in 99.8 % ethanol during 12 h.  
208 Many authors have performed the incubation of electrodes in aqueous solution during 4 or  
209 more hours using various concentrations of cysteamine in aqueous solution [38–43]. There are  
210 also some reports of the gold electrode modification in the ethanolic solution [44,45]. The  
211 previous work proved that there are no significant differences in the formation of monolayer  
212 for the cysteamine dissolved in water or ethanol [46]. The modification of electrodes with  
213 BMS-8 was performed in the anhydrous conditions using DMSO due to the better solubility  
214 of BMS-8 in this solvent. The chemical reaction was carried out by prior activation of BMS-8  
215 carboxylic group performed in the mixture of EDC/NHS [47].

216 The carboxylic group of BMS-8 forms an amide bond with the amine group of  
217 cysteamine anchored on the electrode. It is worth noting that the carboxylic group of BMS-8  
218 is not essential for the interaction of the compound with PD-L1 protein [30]. Therefore, BMS-  
219 8 anchored onto the electrode surface by amide bond maintains its activity.

220 During performed experiments the non-specific binding spots occurring on the surface  
221 of the electrode were not blocked by BSA, however the influence of 1% BSA in 0.01 M PBS,  
222 pH 7.4 on the electrode behavior after modification was also tested. Electrodes obtained in  
223 this procedure were subsequently used to examine various concentrations (in the range of  $10^{-18}$   
224  $10^{-8}$  M) of PD-L1 protein. Each step of electrode preparation and chemical structure of



225 BMS-8 is shown in Figure 1 A. The detection of PD-L1 protein concentration is based on the  
 226 modulated charge transfer kinetics, in presence of the redox species, after PD-L1 is anchored  
 227 on the functionalized electrode surface. All steps of the modification and detection of  
 228 examined proteins were characterized by changes in EIS and CV measurements. The same  
 229 procedure as described above was performed for the study of interaction of obtained  
 230 electrodes with PD-1 protein in the range of concentration from  $10^{-18}$  to  $10^{-8}$  M and BTLA  
 231 and CD 160 in the concentration of  $10^{-8}$  M.



232 Fig 1. A) The picture of gold electrode and the procedure of its modification by cysteamine  
 233 and BMS-8. B) High-resolution XPS spectra obtained in the binding energy range of: (a) *C1s*,  
 234 (b) *O1s*, (c) *S2p*, and (d) *N1s* photopeaks.  
 236

### 3.2. XPS measurements during each step of gold electrode modification process

Figure 1B presents the results of the high-resolution XPS analysis conducted on the surface of functionalized Au electrodes in the energy range of *C1s*, *O1s*, *S2p*, and *N1s* peaks. The analysis was also carried for *Au4f* peak doublet, which served as a reference for the peak calibration and the indicator of the acquired functionalization thickness.

The primary component reported in *C1s* spectrum (Fig. 2a) — *C1s.A* — is located at  $284.6 \pm 0.1$  eV for BMS-8 and PD-L1 samples but exhibits even more positive shift towards 285.1 eV for BSA+PD-L1 samples. The peaks located at this binding energy range are typically attributed to various aliphatic hydrocarbon species but can also originate from adventitious carbon contamination due to air exposure. The second notable component — *C1s.B* — is shifted versus the primary *C1s* component by approx. +1.6 eV and originates from C-O and C-N bonds found in hydroxyls, esters, amines, and others. The last component *C1s.C* was observed at approx. 288.2 eV in an energy range most often associated with carboxyl functional groups. The contribution of the last component is distinctly more prominent for BSA/PD-L1 samples, where its share in total carbon content is approx. 25% versus 15% for PD-L1 samples and 7% for BMS-8. The details of the peak decomposition are summarized in Table 1. The applied model is consistent with numerous literature reports [48–52].

Table 1. Results of high-resolution XPS analysis and peak deconvolution

	<i>C1s</i>			<i>O1s</i>		<i>S2p</i>		<i>N1s</i>	<i>Au4f</i>
	<i>C1s.A</i>	<i>C1s.B</i>	<i>C1s.C</i>	<i>O1s.A</i>	<i>O1s.B</i>	<i>S2p<sub>3/2</sub>.A</i>	<i>S2p<sub>1/2</sub>.B</i>	<i>N1s.A</i>	--
BE / eV	284.6*	286.2	288.2	531.6	532.8	164.5	167.7	399.7**	84.0
<b>BMS-8</b>	41.2	7.6	3.5	3.5	3.7	2.8	1.1	3.5	33.1
<b>BSA/PD-L1</b>	40.2	11.1	11.3	7.0	7.3	1.8	1.0	9.1	11.2
<b>PD-L1</b>	36.7	10.1	5.7	4.0	5.9	2.6	0.9	4.5	29.6

\* *C1s.A* peak was equal 285.0 eV for both BSA/PD-L1 samples.

\*\* *N1s.A* peak was equal 400.2 eV for both BSA/PD-L1 samples.

260 The presence of carbon-oxygen bonds, which are characteristic for organic  
261 compounds, was further confirmed based on *O1s* peak analysis (Fig. 2b) where the presence  
262 of C-O/OH and C=O bonds is reflected in the photopeaks located at *O1s.A* = 531.6 eV and  
263 *O1s.B* = 532.8 eV, respectively. The lowest amount of oxygen in the BMS-8 sample  
264 corresponds to the smallest share of *C1s.B* and *C1s.C* peaks during *C1s* spectra analysis  
265 [53,54]. XPS analysis carried out in the binding energy range of *N1s* photopeak (*N1s.A*)  
266 resulted in the observation of the significant differences between BSA/PD-L1 and the  
267 remaining samples. The *N1s* peak position is shifted by +0.5 eV with respect to BMS-8 and  
268 both PD-L1 samples. The position of this peak is most commonly attributed to N-H and N-C  
269 bonds in amines [55,56]. The energy shift most likely originates from the different number of  
270 carbon atoms adjacent to nitrogen. Indeed, the amount of nitrogen in BSA/PD-L1 samples  
271 was over twice higher than in PD-L1 samples. Higher nitrogen content might also be the  
272 reason of the *C1s.A* component energy shift (*C1s.A'* and *C1s.A''*). Each analyzed sample  
273 contained between 2.5 and 4 at.% of sulfur present in two chemical states. The primary state  
274 marked as *S2p.A* is located in the binding energy characteristic for thiols and other organic  
275 forms of sulfur, while the second component (*S2p.B*) was significantly smaller and shifted  
276 towards BE range typical for sulfates. The XPS analyses allow to bring a conclusion  
277 regarding successful electrode surface functionalization with studied proteins.

278 Finally, the XPS analysis also provides coarse information about the electrode  
279 functionalization thickness. The photoelectrons are emitted only from approximately 5-10 nm  
280 depth underneath the interface. Two conclusions can thus be drawn. First, the  
281 functionalization thickness did not exceed 10 nm in any case, a conclusion drawn based on  
282 the presence of *Au4f* peak doublet for metallic gold in the analyzed surface chemical states.  
283 Second, the functionalization is thinner in the case of BSA/PD-L1 samples.

284

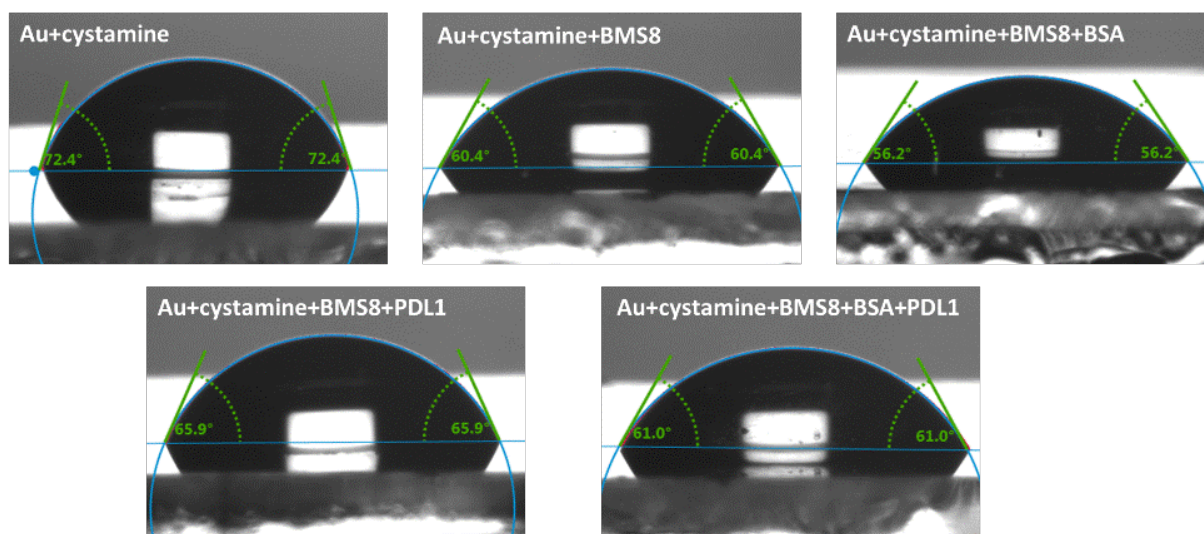




### 285 3.3. Surface wettability measurements

286 In order to assess the hydrophobic and hydrophilic character of the modified surface at  
287 the different steps of the modification process of the gold electrodes, contact angles of water  
288 drops deposited on the surfaces were measured (Fig 2, Fig. 3a). For gold electrodes the water  
289 contact angle decreased after modification with cysteamine for about 10°. Further  
290 modification with BMS-8 led to a decrease in the contact angle for about 12°. The decrease of  
291 contact angle on the modified Au electrodes revealed an increase of hydrophilic character of  
292 the surface because of the functional groups present in the modified layer. Deposition of BSA  
293 on the modified layer leads to another decrease in the contact angle for about 5°. In both cases  
294 (with or without the BSA) after exposure to the PD-L1 protein an increase in the contact angle  
295 is observed, hence the hydrophobicity of the layer increases (Fig 2, Table S2).

296



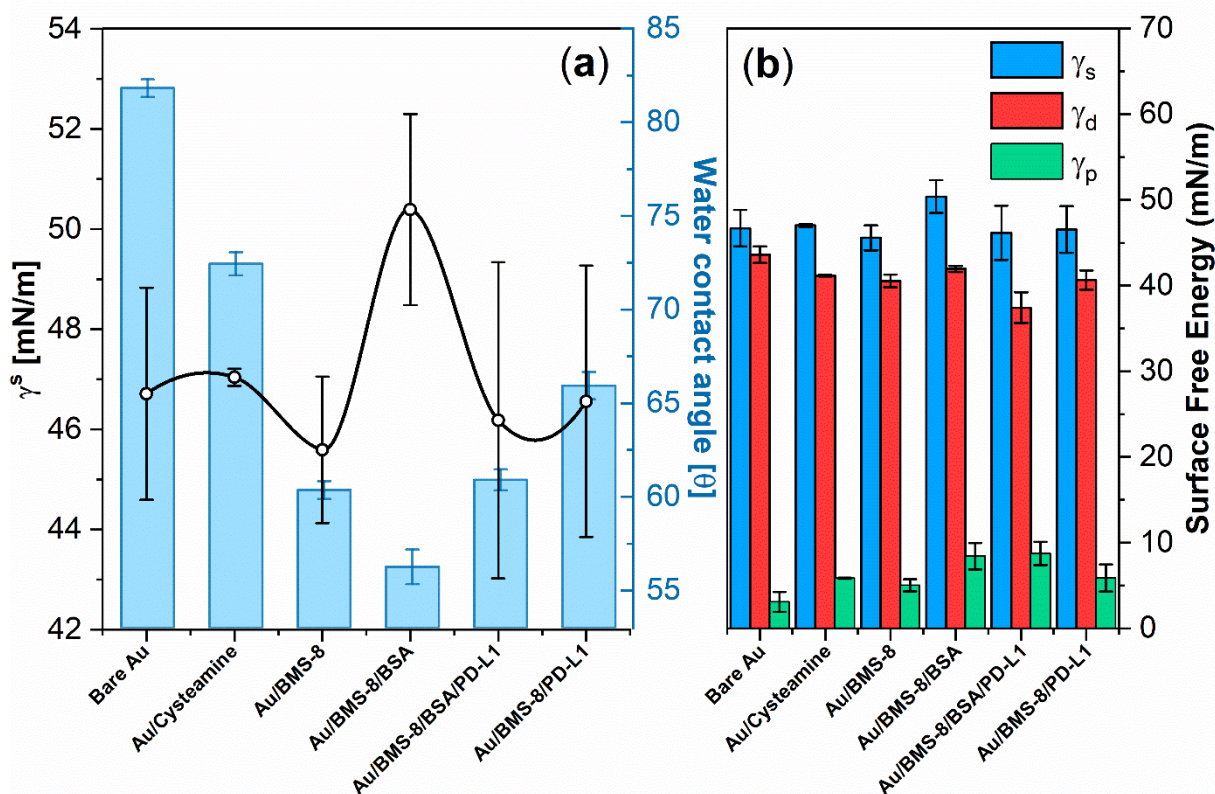
297  
298 **Fig. 2.** Photos of the water contact angle measurements for each step of gold electrode  
299 modification for PD-L1 sensing.

300  
301 Considering the changes in SFE energy in relation to the subsequent stages of  
302 modification, the total free energy does not change significantly as to the value, while the  
303 changes in the chemical structure of the layer also change the SFE value (Fig. 3b). The total

304 SFE and its polar component increased as a result of the incorporation of more functional  
305 polar groups due to the modification process. Changes in the free energy of the surface are  
306 mainly the effect of the change of the polar component, while the dispersion part remains  
307 essentially unchanged.

308         Already the first stage of modification with cysteamine causes the increase of the  
309 acid-base component from 3.09 mN/m to 5.86 mN/m. Furthermore, the acidic and basic  
310 elements of the polar component undergo a complete change. In the case of an unmodified  
311 electrode, the acid component has a much higher share. The modification process not only  
312 lowers their values but also reverses the proportions — the basic component is now dominant.  
313 This is probably consistent with the presence of amino groups exhibiting basic properties on  
314 the electrode surface. The largest increase in the basic component is observed in the case of  
315 BMS-8/BSA and BMS-8/BSA/PD-L1 samples. This observation is consistent with the results  
316 obtained from the XPS measurements which indicated these samples as containing the most  
317 nitrogen atoms in the form of different types of amino groups.





318

319 Fig. 3.a) Water contact angle and b) SFE energy  $\gamma_s$  diagram with uncertainties for each step of  
 320 the modification of the gold electrode for PD-L1 sensing.

321

322 This variability affects the hydrophilicity of the surface and thus the observed contact angle.

323 The most hydrophilic surfaces are observed for BMS-8/BSA and BMS-8/BSA/PD-L1

324 samples. Their water contact angle (WCA) decreased from 81.82 for unmodified gold

325 electrode to 56.26 and 60.90 for BMS-8/BSA and BMS-8/BSA/PD-L1, respectively.

326

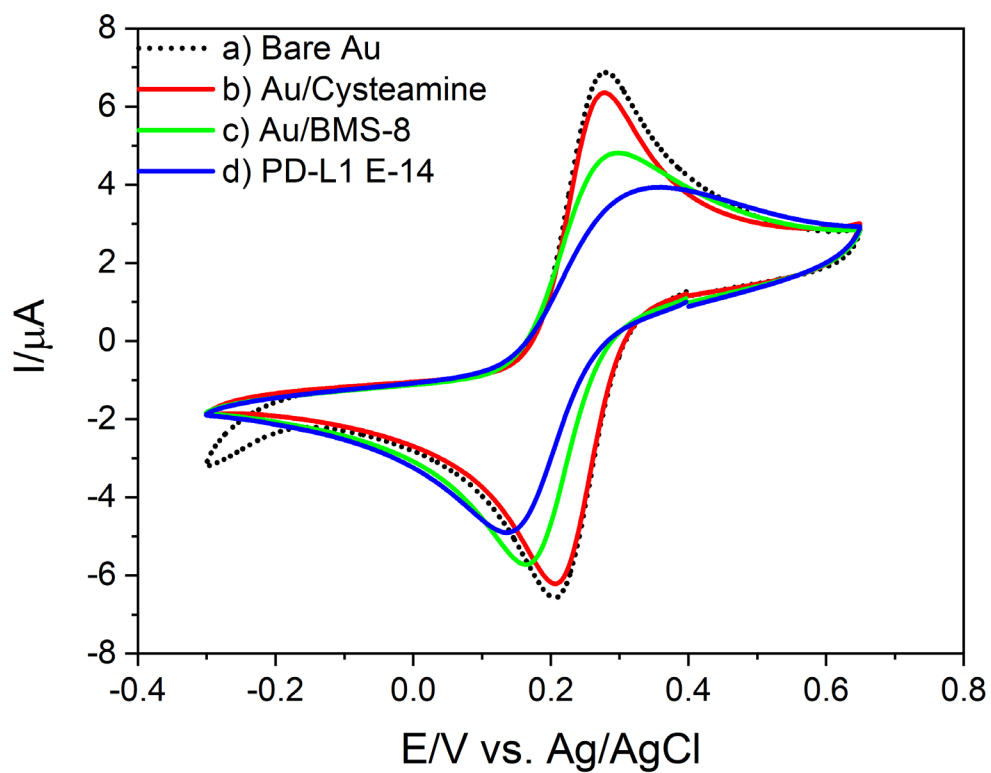
### 327 3.4. Electrochemical measurements

328 The cyclic voltammetry measurements were performed during each step of electrodes  
329 modification in 0.1 M of PBS, pH 7.0 containing 1 mM  $\text{Fe}[(\text{CN})_6]^{3-/4-}$ . The results of CV  
330 measurements show two reversible peaks for bare Au electrodes, where the ratio of anodic  
331 peak to cathodic peak current  $i_A/i_C$  is close to 1 with the peak-to-peak separation ( $\Delta E$ ) of 67  
332 mV (Fig. 4. black dotted line). After modification by cysteamine, the peak-to-peak separation  
333  $\Delta E$  decreased to 64 mV and is similar to those calculated for bare Au electrodes. Therefore, a  
334 conclusion may be drawn that cysteamine modification of Au electrodes does not influence  
335 significantly its electrochemical behavior, which was also confirmed in our measurements by  
336 EIS technique. The voltammogram is shifted towards more negative potential after  
337 modification, a feature observed before [44].

338 The modification with BMS-8 caused the peak currents to decrease and the increase of  
339 peak-to-peak separation to 119 mV. In the next step, such modified electrode was incubated  
340 with PD-L1 protein in a concentration of  $10^{-14}$  M. The changes of obtained voltammograms  
341 are significant. The peak current values decreased, and the peak-to-peak separation increased,  
342  $\Delta E$  to 180 mV (Fig. 4), as an effect of PD-L1 anchoring at the modified electrode surface and  
343 affecting the charge transfer kinetics by the redox species. This particular behavior of the  
344 modified electrodes is probably the consequence of two competitive factors: partial blockage  
345 of active sites at the electrode and electrostatic interactions between PD-L1 protein and  
346 negatively charged ions  $\text{Fe}[(\text{CN})_6]^{3-/4-}$  present in the examined solution [55,56].

347 The experiment was performed using gold electrode modified by cysteamine with  
348 BMS-8 without incubation with 1% BSA in 0.01 M PBS due to the small changes caused by  
349 BSA observed in electrode response in previous experiments (see Fig. S1). Above experiment  
350 directly confirm that gold electrode modified by BMS-8 is highly sensitive to PD-L1 protein  
351 present in solution.





352

353 **Fig. 4.** Cyclic voltammograms of the redox reaction of 1 mM  $\text{Fe}[(\text{CN})_6]^{3-/4-}$  in 0.1 M PBS, pH  
 354 7.0 solution obtained at a) Bare Au b) Au/Cysteamine c) Au/BMS-8 d) Au/BMS-8/PD-L1  
 355 electrode, scan rate 100 mV/s.

356 Next, the electrochemical impedance spectroscopy measurements have been  
357 performed to determine the capability of the obtained electrodes for detecting PD-L1 at very  
358 low concentrations. Additionally, the electrodes modified with BMS-8 were used as a control  
359 test during PD-1 detection. The impedance approach offers significantly higher sensitivity for  
360 the determination of electrode kinetics changes in comparison with CV measurements.  
361 Therefore, it was selected for the evaluation of both PD-L1 and PD-1 concentrations in the  
362 same range of  $10^{-18}$  to  $10^{-8}$  M. Figure 4 presents the EIS impedance spectra for the bare Au  
363 electrodes in 0.1 M PBS pH 7.0 solution containing 1 mM  $\text{Fe}[(\text{CN})_6]^{3-/4-}$ , after consecutive  
364 surface modification steps and after incubation in solution containing PD-L1 protein in  
365 concentration range of  $10^{-8}$  to  $10^{-18}$ .

366 The shape of the impedance spectra is characterized by the semicircle at the high-to-  
367 moderate frequency range and very distinctive feature in the form of solid line inclined at  $45^\circ$   
368 at low-frequency range. The discussed feature should be associated with the diffusion-related  
369 impedance and testifies for the co-occurrence of the diffusion control in the charge-transfer  
370 process. On the other hand, it is clearly visible in the inset of Fig. 5 that the next electrode  
371 modification steps influence the electrode's charge transfer resistance as observed through the  
372 increase of the high-frequency semicircle.

373 The electric equivalent circuit (EEC) was selected based on the obtained impedance  
374 studies. The EEC with abbreviated notation  $R(Q(RW))$  is composed of R - solution resistance  
375 and a parallel connection of the constant phase element (CPE), imitating the heterogeneities at  
376 the electrode surface and charge transfer resistance  $R_{CT}$  with Warburg diffusion resistance W  
377 (Fig. 5). The impedance of the CPE is given with eq. (1)

$$378 \quad Z_{CPE} = \frac{1}{Q(j\omega)^\alpha} \quad (1)$$

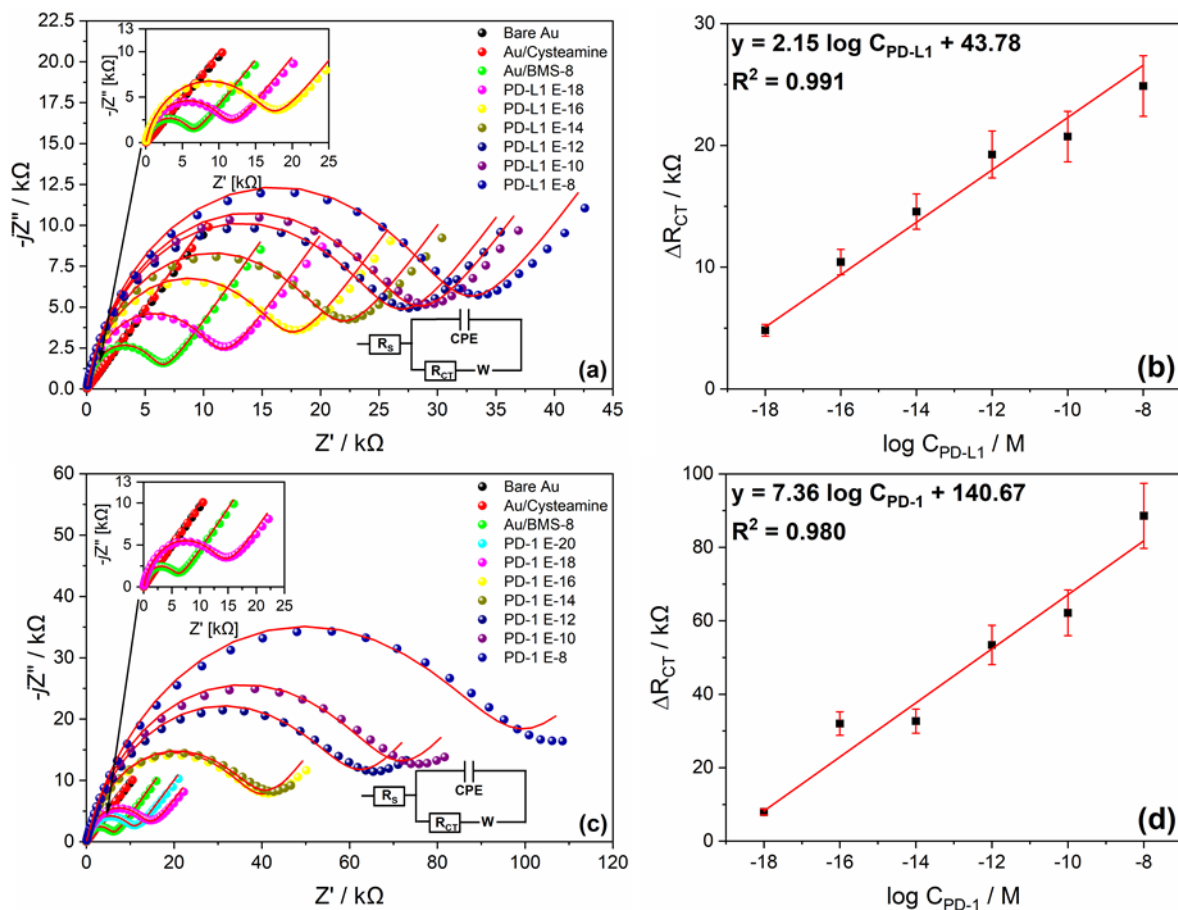
379 where Q is the quasi-capacitance in the presence of frequency dispersion of capacitance, CPE  
380 exponent  $\alpha$  is the heterogeneity factor,  $j$  is the imaginary number and  $\omega$  is the angular

381 frequency [57–62]. CPE exponent  $\alpha$  is often considered to be the surface heterogeneity factor  
382 ( $0 < \alpha < 1$ ). The closer to unity  $\alpha$  approaches, the more closely the CPE resembles a pure  
383 double-layer capacitance, and if  $\alpha$  approaches 0, the CPE behaves more like a resistor. The  
384 above-defined heterogeneity may be introduced by numerous features, including non-uniform  
385 site-specific charge transfer kinetics due to electrode polycrystallinity, 2D adsorption of  
386 macromolecules or contaminants, and resultant interspace regions but also electrode material  
387 geometry and porosity [63–69]. The utilization of such electric equivalent circuit is explained  
388 due to the large molecular mass of examined proteins and is widely used for the gold  
389 electrode modified by cysteamine and other organic molecules [70–74]. The EEC allowed  
390 obtaining a very good fit as represented by  $\chi^2$  distribution about  $10^{-4}$ . The more detailed  
391 analyses of are summarized in Table S3 in Supporting Information file.

392         The impedance spectra for both: bare Au electrode and Au after modification with  
393 cysteamine reveal nearly straight line at  $45^\circ$  (Fig. 5a inset), a feature characteristic for a mass  
394 diffusion limiting the electron transfer process. The electrode modification through a chemical  
395 reaction between electrode-terminating amine functional groups with the carboxyls within  
396 BMS-8 molecule caused the appearance of a distinctive capacitive semicircle on the  
397 impedance spectra, indicating the formation of the adsorbed layer, which influence the  
398 interfacial electron transfer.

399         The BMS-8 surface functionalization process occurs with different efficiency for  
400 various electrodes, differing in BMS-8 anchoring density, resulting in differences in layer  
401 thickness, and subtle Au pretreatment conditions, etc. These features have a non-negligible  
402 influence on the kinetics of the charge transfer through the electrode interface. Therefore, in  
403 order to efficiently verify the effect of anchoring the PD-L1 molecule on the modified  
404 electrode surface, it is essential to perform the experiment on a single electrode, to be able to  
405 observe the relative changes of  $R_{CT}$  parameter. The relative change of the charge transfer

406 resistance was calculated according to the equation:  $\Delta R_{CT} = R_{CT(PD-L1)} - R_{CT(BMS-8)}$ , where  
 407  $R_{CT(BMS-8)}$  is a value of  $R_{CT}$  of electrode modified by BMS-8 and  $R_{CT(PD-L1)}$  is  $R_{CT}$  after  
 408 incubation in different concentration of PD-L1. The obtained results are shown in Fig. 5b.



409  
 410 **Fig. 5.** The EIS impedance spectra of BMS-8 functionalized electrode in the absence and the  
 411 presence of a) PD-L1 and c) PD-1 protein in 0.01 M PBS, pH 7.0 at various concentrations  
 412 ratio from  $10^{-18}$  M to  $10^{-8}$  M. In the inset enlarged the comparison of obtained spectra for a)  
 413 PD-L1 and c) PD-1 concentration of  $10^{-18}$  M. Points represent experimental results while solid  
 414 red line represent data calculated using EEC.  
 415 The calibration curve for the  $\Delta R_{CT}$  changes resulting from b) PD-L1 and d) PD-1 protein  
 416 exposure of the electrode as a function of logarithmic concentration of PD-L1.  
 417

418 It is clearly visible that tested BMS-8 deposited at the Au electrode surface is highly  
 419 sensitive, differentiating impedance characteristics of the electrode even at the lowest studied  
 420 concentration of PD-L1. These results indicate that studied protein binds to the BMS-8  
 421 molecules, anchored on the Au electrode. The increasing protein concentration causes  
 422 inhibition of the charge transfer process, resulting in  $R_{CT}$  increase. The observed behavior

423 corresponds with the formation of the functionalized organic layer affecting the charge  
424 transfer kinetics. The EIS studies revealed that the  $R_{CT}$  of the above-functionalized electrode  
425 increases over 2.5 times in the presence of PD-L1 protein in the vicinity in the concentration  
426 of  $10^{-18}$  M to  $10^{-8}$  respectively (Table S4).

427 Performing the above-described  $R_{CT}$  normalization allowed us to form the calibration  
428 curve, thus offering the detection tool of ultra-small PD-L1 concentrations on the modified  
429 Au surface, based on electrochemical impedance measurements. The electrochemical  
430 response of the BMS-8 modified gold electrode was linear in the entire range of the PD-L1  
431 from  $10^{-8}$  M to  $10^{-18}$  M. The calculated regression equation was:  $\Delta R_{CT} = 2.15 \log C[\text{PD-L1}] +$   
432  $43.78$  with the correlation coefficient of 0.991. The detection limit (LOD) was estimated to be  
433  $1.87 \times 10^{-14}$  M and  $2.93 \times 10^{-14}$  M for PD-L1 and PD-1 (S/N=3.3) respectively, while the limit  
434 of quantification (LOQ) was calculated to be  $5,67 \times 10^{-14}$  M for PD-L1 and  $8,87 \times 10^{-14}$  M for  
435 PD-L1.

436

### 437 ***3.6. Specificity and selectivity of the impedance PD-L1 assay***

438 In order to examine the selectivity of the above-presented approach, the same  
439 experiment was performed towards the detection of the PD-1 protein. Obtained results  
440 confirm that the presence of PD-1 protein in the analyte has a visible effect on the charge  
441 transfer, increasing  $R_{CT}$  (Fig. 5c). The results of impedance analyses of PD-1 protein detection  
442 are summarized in Table S3. The data plotted in Fig. 5d reveals that the  $\Delta R_{CT}$  changes  
443 recorded for the Au/BMS-8 were linear in the range of analyzed PD-1 concentrations, similar  
444 as in the case of PD-L1 protein. The estimated regression equation was  $\Delta R_{CT} = 7.36 \log$   
445  $C[\text{PD-1}] + 140.67$ , with the correlation coefficient equal to 0.980 (Fig. 5d). BMS-8  
446 functionalized electrode response to PD-1 is unexpected given the fact that BMS-8 was shown

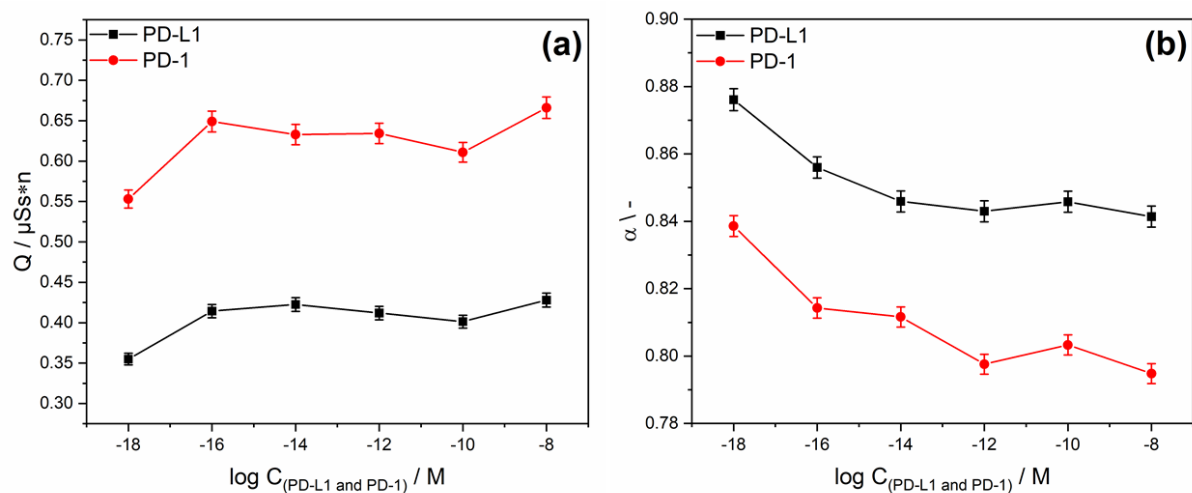


447 not to interact with PD-1 [28]. Likely the surface modification process itself provides anchor  
448 points for PD-1.

449 The performed analyses directly indicate the linear trend of  $\Delta R_{CT}$  change as a function  
450 of target protein concentration for both studied proteins. However, there is also a significant  
451 difference in the slope of the linear function. The charge transfer resistance through the BMS-  
452 8-modified Au electrode increases over 2.5 times in the analyzed concentration range of PD-  
453 L1, and over 5.0 times in the same range of PD-1 protein. Thus, a conclusion should be drawn  
454 that analysis of this one parameter allows for an ultrasensitive quantitative analysis but does  
455 not allow for qualitative analysis distinguishing between PD-1 and PD-L1 proteins.

456 There are, however, other parameters obtained based on the impedance analyses. An  
457 important feature should be observed when analyzing the changes of the quasi-capacitive  
458 parameter with the concentration change of either PD-1 or PD-L1 molecules, the results of  
459 which are presented in Fig. 6.

460



461  
462 **Fig. 6.** a) The relationship of a) quasi-capacitance in the presence of frequency dispersion of  
463 capacitance (Q) and b) heterogeneity factor ( $\alpha$ ) as a function of logarithmic concentration of  
464 PD-L1 and PD-1 proteins.  
465



466 The quasi-capacitance parameter  $Q_{DL}$  increases with analyte concentration for both  
467 studied proteins PD-L1 and PD-1, and this effect is strongly correlated with the decrease in  
468 CPE exponent  $\alpha$ , indicating a slight decrease in electrode homogeneity when more and more  
469 target proteins are anchored on the electrode surface. This is an expected and valuable result,  
470 confirming the correct selection of the EEC.

471 The values of the quasi-capacitance of the modified Au electrode exposed to the  
472 studied proteins differ significantly. The heterogeneity introduced by the PD-L1 molecule is  
473 significantly smaller than the heterogeneity introduced by the PD-1 molecules (higher  $\alpha$   
474 values for PD-L1). BMS-8 interacts more specifically with PD-L1 than with PD-1. More  
475 homogeneous surface distribution of the adsorption layer in case of PD-L1 may be caused by  
476 formation of homodimer on the electrode surface. Inducing dimerization of PD-L1 protein  
477 after interaction with BMS-8 was confirmed by X-ray [30]. On the other hand, experimental  
478 data indicate that BMS-8 compound does not bind to PD-1 protein [75]. PD-1 protein also  
479 interacts with the electrode, but as a result, the electrode surface is more heterogeneous. Most  
480 likely, the interaction of the PD-1 with a modified electrode is probably non-specific and  
481 random.

482 The higher the protein concentration the lower the electric homogeneity at the  
483 electrode/electrolyte interface. However, the homogeneity level obtained in the case of  
484 anchored PD-L1 proteins at the highest studied concentration  $10^{-8}$  M is unattainable for PD-1,  
485 even at the lowest studied concentrations. These differences translate into significant  
486 differences between quasi-capacitance of PD-L1 and PD-1 films at the modified electrode  
487 surface and demonstrate that BMS-8 strongly and specifically interacts with PD-L1 protein,  
488 offering possible routes for PD-L1 assay selectivity in presence of other proteins. The  
489 comprehensive impedance analysis allows to qualitatively distinguish PD-L1 and PD-1



490 proteins and provide ultrasensitive quantitative information regarding target protein  
491 concentration.

492 These results are in good agreement with previous studies by the Holak and co-  
493 workers, who show that BMS-8 leads to dissociation of PD-1/PD-L1 complex and induction  
494 of PD-L1 protein dimerization [28,76]. The interaction of BMS-8 with PD-L1 partially  
495 overlaps the hydrophobic interaction surface between PD-1 protein and its ligand, PD-L1.  
496 Furthermore, the formation of the homodimer limits access of the PD-1 receptor to the  
497 binding site of PD-L1 protein [75–77].

498 Besides of PD-L1 and PD-1 examination, the electrochemical response of other  
499 proteins was also investigated to evaluate the electrochemical behavior of the modified  
500 electrode on the selectivity of protein detection. For this purpose, we selected CD160, and  
501 BTLA proteins that belong to the immunoglobulin-like proteins superfamily (IgSF), the same  
502 as PD-L1 and PD-1 [78,79]. It is worth noting that the interaction studies of the BMS-8  
503 molecule with the PD-1 protein have been carried out and the results have shown that BMS-8  
504 binds to PD-L1 but not to PD-1 [28]. In vitro NMR measurements presents that BMS-8 is  
505 capable of dissociating the PD-1/PD-L1 interaction in the stoichiometric concentration [75].  
506 The same studies for CD160 and BTLA were not performed. In presented studies, the EIS  
507 impedance of selected proteins in 0.01 M PBS, pH 7.0 at concentration of  $10^{-8}$  M was  
508 measured. The impedance results in the form of Nyquist plots are shown in Figure S4.

509 Presented studies show that the functionalized electrodes bind the CD160 and BTLA  
510 proteins to the anchored BMS-8 but with significantly less potency than the PD-L1 and PD-1  
511 proteins (Fig. S4). The results of the impedance analysis using  $R(Q(RW))$  EEC are  
512 summarized in Table S5.



### 513 3. Conclusions

514 Summarizing, this work is focused on designing new assay capable to detect cancer marker,  
515 sPD-L1 protein, in low concentration using EIS and CV. It describes the development of the  
516 new electrode functionalization, which is capable of PD-L1 detection in PBS solution. The  
517 applied approach utilizes the reaction of BMS-8 with cysteamine anchored at gold electrode  
518 surface. Performed high-resolution XPS, contact angle, and surface free energy studies  
519 confirmed each successful step of the electrode modification. Cyclic voltammetry confirmed  
520 the detection of PD-L1 protein in the concentration of  $10^{-14}$  M, while the electrochemical  
521 impedance spectroscopy performed at various concentrations in the range of  $10^{-18}$  to  $10^{-8}$  M.  
522 We have proved the efficient both PD-L1 as well as PD-1 detection through change in charge  
523 transfer resistance  $R_{CT}$  even at its lowest concentration of  $10^{-18}$  M. Subsequently, it should be  
524 noted that the changes in the electric parameters with PD-L1 and PD-1 concentration show a  
525 linear trend, significantly enabling quantitative analysis with the low detection limit of  $1.87 \times$   
526  $10^{-14}$  for PD-L1 M and  $2.93 \times 10^{-14}$  M for and PD-1 respectively. While offering ultrasensitive  
527 protein detection, the  $R_{CT}$  analysis does not allow for selective PD-L1 or PD-1 protein  
528 determination, since the assay is affected by both proteins. Likely, interaction with PD-L1 is  
529 BMS-8 specific while that with PD-1 is guided by less defined surface effects at the  
530 functionalized electrode. We claim that the selectivity of the proposed assay may be based on  
531 quasi-capacitance parameter analysis. Smaller decrease of electrode homogeneity for PD-  
532 L1/BMS-8 interaction in comparison to PD-1/BMS-8 can be explained by dimerization of  
533 PD-L1 protein induced by BMS-8 which not occur in case of PD-1/BMS-8. The constant  
534 phase element parameters  $Q$  and  $\alpha$  show that it is possible to differentiate PD-L1 from PD-1  
535 protein and it will be investigating further in more complex mixtures e.g. animal or human  
536 serum. Our studies confirmed that immune checkpoint proteins CD160 and BTLA anchor at  
537 the electrode with significantly less potency than the PD-L1.

538

539 **Acknowledgments**

540           This work was financially supported by Polish National Science Centre (NCN) under  
541 Grant No. 2015/17/D/ST5/02571 (J.R.), Grant No. 2017/25/B/NZ1/00827 (G.D.) and by  
542 Polpharma Scientific Foundation Grant No. 3/XVIII/2019 (S.R.-M.).

- 544 [1] F. Bray, J. Ferlay, I. Soerjomataram, R.L. Siegel, L.A. Torre, A. Jemal, Global cancer  
545 statistics 2018: GLOBOCAN estimates of incidence and mortality worldwide for 36 cancers  
546 in 185 countries, *CA: A Cancer Journal for Clinicians*. 68 (2018) 394–424.  
547 <https://doi.org/10.3322/caac.21492>.
- 548 [2] S. Mehta, A. Shelling, A. Muthukaruppan, A. Lasham, C. Blenkiron, G. Laking, C.  
549 Print, Predictive and prognostic molecular markers for cancer medicine, *Ther Adv Med*  
550 *Oncol.* 2 (2010) 125–148. <https://doi.org/10.1177/1758834009360519>.
- 551 [3] R.C. Dolscheid-Pommerich, M. Keyver-Paik, T. Hecking, W. Kuhn, G. Hartmann, B.  
552 Stoffel-Wagner, S. Holdenrieder, Clinical performance of LOCI<sup>TM</sup>-based tumor marker  
553 assays for tumor markers CA 15-3, CA 125, CEA, CA 19-9 and AFP in gynecological  
554 cancers, *Tumour Biol.* 39 (2017) 1010428317730246.  
555 <https://doi.org/10.1177/1010428317730246>.
- 556 [4] I. Jacobs, R.C. Bast, The CA 125 tumour-associated antigen: a review of the literature,  
557 *Hum Reprod.* 4 (1989) 1–12. <https://doi.org/10.1093/oxfordjournals.humrep.a136832>.
- 558 [5] P.M. Göcze, D.G. Szabó, G.N. Than, I.F. Csaba, K.F. Krommer, Occurrence of CA  
559 125 and CA 19-9 Tumor-Associated Antigens in Sera of Patients with Gynecologic,  
560 Trophoblastic, and Colorectal Tumors, *GOI.* 25 (1988) 268–272.  
561 <https://doi.org/10.1159/000293797>.
- 562 [6] X. Frigola, B.A. Inman, C.J. Krco, X. Liu, S.M. Harrington, P.A. Bulur, A.B. Dietz,  
563 H. Dong, E.D. Kwon, Soluble B7-H1: Differences in production between dendritic cells and  
564 T cells, *Immunology Letters.* 142 (2012) 78–82. <https://doi.org/10.1016/j.imlet.2011.11.001>.
- 565 [7] J. Zhou, K.M. Mahoney, A. Giobbie-Hurder, F. Zhao, S. Lee, X. Liao, S. Rodig, J. Li,  
566 X. Wu, L.H. Butterfield, M. Piesche, M.P. Manos, L.M. Eastman, G. Dranoff, G.J. Freeman,  
567 F.S. Hodi, Soluble PD-L1 as a biomarker in malignant melanoma and checkpoint blockade,  
568 *Cancer Immunol Res.* (2017) canimm.0329.2016. <https://doi.org/10.1158/2326-6066.CIR-16-0329>.
- 570 [8] X. Bi, H. Wang, W. Zhang, J. Wang, W. Liu, Z. Xia, H. Huang, W. Jiang, Y. Zhang,  
571 L. Wang, PD-L1 is upregulated by EBV-driven LMP1 through NF- $\kappa$ B pathway and correlates  
572 with poor prognosis in natural killer/T-cell lymphoma, *Journal of Hematology & Oncology.* 9  
573 (2016) 109. <https://doi.org/10.1186/s13045-016-0341-7>.
- 574 [9] T. Nagato, T. Ohkuri, K. Ohara, Y. Hirata, K. Kishibe, Y. Komabayashi, S. Ueda, M.  
575 Takahara, T. Kumai, K. Ishibashi, A. Kosaka, N. Aoki, K. Oikawa, Y. Uno, N. Akiyama, M.  
576 Sado, H. Takei, E. Celis, Y. Harabuchi, H. Kobayashi, Programmed death-ligand 1 and its  
577 soluble form are highly expressed in nasal natural killer/T-cell lymphoma: a potential  
578 rationale for immunotherapy, *Cancer Immunol Immunother.* 66 (2017) 877–890.  
579 <https://doi.org/10.1007/s00262-017-1987-x>.
- 580 [10] D. Rossille, M. Gressier, D. Damotte, D. Maucort-Boulch, C. Pangault, G. Semana, S.  
581 Le Gouill, C. Haioun, K. Tarte, T. Lamy, N. Milpied, T. Fest, Groupe Ouest-Est des  
582 Leucémies et Autres Maladies du Sang, Groupe Ouest-Est des Leucémies et Autres Maladies  
583 du Sang, High level of soluble programmed cell death ligand 1 in blood impacts overall  
584 survival in aggressive diffuse large B-Cell lymphoma: results from a French multicenter  
585 clinical trial, *Leukemia.* 28 (2014) 2367–2375. <https://doi.org/10.1038/leu.2014.137>.
- 586 [11] L. Wang, H. Wang, H. Chen, W. Wang, X. Chen, Q. Geng, Z. Xia, Y. Lu, Serum  
587 levels of soluble programmed death ligand 1 predict treatment response and progression free  
588 survival in multiple myeloma, *Oncotarget.* 6 (2015) 41228–41236.  
589 <https://doi.org/10.18632/oncotarget.5682>.
- 590 [12] X. Frigola, B.A. Inman, C.M. Lohse, C.J. Krco, J.C. Cheville, R.H. Thompson, B.C.  
591 Leibovich, M.L. Blute, H. Dong, E.D. Kwon, Identification of a Soluble Form of B7-H1 That

- 592 Retains Immunosuppressive Activity and Is Associated with Aggressive Renal Cell  
593 Carcinoma, *Clin Cancer Res.* (2011) clincanres.0250.2010. <https://doi.org/10.1158/1078->  
594 0432.CCR-10-0250.
- 595 [13] S. Kitano, T. Nakayama, M. Yamashita, Biomarkers for Immune Checkpoint  
596 Inhibitors in Melanoma, *Front. Oncol.* 8 (2018). <https://doi.org/10.3389/fonc.2018.00270>.
- 597 [14] S.P. Patel, R. Kurzrock, PD-L1 Expression as a Predictive Biomarker in Cancer  
598 Immunotherapy, *Mol Cancer Ther.* 14 (2015) 847–856. <https://doi.org/10.1158/1535->  
599 7163.MCT-14-0983.
- 600 [15] J.T. Jørgensen, K.B. Nielsen, Companion and complementary diagnostics for first-line  
601 immune checkpoint inhibitor treatment in non-small cell lung cancer, *Transl Lung Cancer*  
602 *Res.* 7 (2018) S95–S99. <https://doi.org/10.21037/tlcr.2018.02.08>.
- 603 [16] C. Teixidó, N. Vilariño, R. Reyes, N. Reguart, PD-L1 expression testing in non-small  
604 cell lung cancer, *Ther Adv Med Oncol.* 10 (2018) 1758835918763493.  
605 <https://doi.org/10.1177/1758835918763493>.
- 606 [17] M. Yi, D. Jiao, H. Xu, Q. Liu, W. Zhao, X. Han, K. Wu, Biomarkers for predicting  
607 efficacy of PD-1/PD-L1 inhibitors, *Molecular Cancer.* 17 (2018) 129.  
608 <https://doi.org/10.1186/s12943-018-0864-3>.
- 609 [18] J. He, Y. Pan, Y. Guo, B. Li, Y. Tang, Study on the Expression Levels and Clinical  
610 Significance of PD-1 and PD-L1 in Plasma of NSCLC Patients, *Journal of Immunotherapy.*  
611 43 (2020) 156–164. <https://doi.org/10.1097/CJI.0000000000000315>.
- 612 [19] J. Zhou, K.M. Mahoney, A. Giobbie-Hurder, F. Zhao, S. Lee, X. Liao, S. Rodig, J. Li,  
613 X. Wu, L.H. Butterfield, M. Piesche, M.P. Manos, L.M. Eastman, G. Dranoff, G.J. Freeman,  
614 F.S. Hodi, Soluble PD-L1 as a biomarker in malignant melanoma and checkpoint blockade,  
615 *Cancer Immunol Res.* (2017) canimm.0329.2016. <https://doi.org/10.1158/2326-6066.CIR-16->  
616 0329.
- 617 [20] D. Rossille, M. Gressier, D. Damotte, D. Maucourt-Boulch, C. Pangault, G. Semana, S.  
618 Le Gouill, C. Haioun, K. Tarte, T. Lamy, N. Milpied, T. Fest, Groupe Ouest-Est des  
619 Leucémies et Autres Maladies du Sang, Groupe Ouest-Est des Leucémies et Autres Maladies  
620 du Sang, High level of soluble programmed cell death ligand 1 in blood impacts overall  
621 survival in aggressive diffuse large B-Cell lymphoma: results from a French multicenter  
622 clinical trial, *Leukemia.* 28 (2014) 2367–2375. <https://doi.org/10.1038/leu.2014.137>.
- 623 [21] L. Wang, H. Wang, H. Chen, W. Wang, X. Chen, Q. Geng, Z. Xia, Y. Lu, Serum  
624 levels of soluble programmed death ligand 1 predict treatment response and progression free  
625 survival in multiple myeloma, *Oncotarget.* 6 (2015) 41228–41236.  
626 <https://doi.org/10.18632/oncotarget.5682>.
- 627 [22] Y. Li, Y. Li, Y. Xiao, Y. Xiao, M. Su, M. Su, R. Zhang, R. Zhang, J. Ding, J. Ding, X.  
628 Hao, X. Hao, Y. Ma, Y. Ma, Role of soluble programmed death-1 (sPD-1) and sPD-ligand 1  
629 in patients with cystic echinococcosis, *Experimental and Therapeutic Medicine.* 11 (2016)  
630 251–256. <https://doi.org/10.3892/etm.2015.2876>.
- 631 [23] L.S. Chupak, M. Ding, S.W. Martin, X. Zheng, P. Hewawasam, T.P. Connolly, N. Xu,  
632 K.-S. Yeung, J. Zhu, D.R. Langle, D.J. TENNEY, P.M. Scola, Compounds useful as  
633 immunomodulators, WO2015160641A2, 2015.  
634 <https://patents.google.com/patent/WO2015160641A2/en?q=WO+2015%2f160641+A2.+W>  
635 [O+2015%2f160641+A2](https://patents.google.com/patent/WO2015160641A2/en?q=WO+2015%2f160641+A2.+W) (accessed January 18, 2019).
- 636 [24] L.S. Chupak, X. Zheng, Compounds useful as immunomodulators,  
637 WO2015034820A1, 2015.  
638 <https://patents.google.com/patent/WO2015034820A1/en?q=WO+2015%2f034820+A1.+W>  
639 [O2015034820+A1](https://patents.google.com/patent/WO2015034820A1/en?q=WO+2015%2f034820+A1.+W) (accessed January 18, 2019).
- 640 [25] M.J. Aghajani, T.L. Roberts, T. Yang, C.E. McCafferty, N.J. Caixeiro, P. DeSouza, N.  
641 Niles, Elevated levels of soluble PD-L1 are associated with reduced recurrence in papillary



- 642 thyroid cancer, *Endocrine Connections*. 8 (2019) 1040–1051. [https://doi.org/10.1530/EC-19-](https://doi.org/10.1530/EC-19-0210)  
643 0210.
- 644 [26] Y. Ding, C. Sun, J. Li, L. Hu, M. Li, J. Liu, L. Pu, S. Xiong, The Prognostic  
645 Significance of Soluble Programmed Death Ligand 1 Expression in Cancers: A Systematic  
646 Review and Meta-analysis, *Scandinavian Journal of Immunology*. 86 (2017) 361–367.  
647 <https://doi.org/10.1111/sji.12596>.
- 648 [27] X. Wu, L. Xu, Q. Cheng, L. Nie, S. Zhang, Y. Du, J. Xue, Increased serum soluble  
649 programmed death ligand 1(sPD-L1) is associated with the presence of interstitial lung  
650 disease in rheumatoid arthritis: A monocentric cross-sectional study, *Respiratory Medicine*.  
651 166 (2020) 105948. <https://doi.org/10.1016/j.rmed.2020.105948>.
- 652 [28] L. Skalniak, K.M. Zak, K. Guzik, K. Magiera, B. Musielak, M. Pachota, B. Szelazek,  
653 J. Kocik, P. Grudnik, M. Tomala, S. Krzanik, K. Pyrc, A. Dömling, G. Dubin, T.A. Holak,  
654 Small-molecule inhibitors of PD-1/PD-L1 immune checkpoint alleviate the PD-L1-induced  
655 exhaustion of T-cells, *Oncotarget*. 8 (2017) 72167–72181.  
656 <https://doi.org/10.18632/oncotarget.20050>.
- 657 [29] U. Jarocka, R. Sawicka, A. Góra-Sochacka, A. Sirko, W. Zagórski-Ostoja, J. Radecki,  
658 H. Radecka, Electrochemical immunosensor for detection of antibodies against influenza A  
659 virus H5N1 in hen serum, *Biosensors and Bioelectronics*. 55 (2014) 301–306.  
660 <https://doi.org/10.1016/j.bios.2013.12.030>.
- 661 [30] K.M. Zak, P. Grudnik, K. Guzik, B.J. Zieba, B. Musielak, A. Dömling, G. Dubin, T.A.  
662 Holak, Structural basis for small molecule targeting of the programmed death ligand 1 (PD-  
663 L1), *Oncotarget*. 7 (2016) 30323–30335. <https://doi.org/10.18632/oncotarget.8730>.
- 664 [31] A. Zielinski, M. Cieslik, M. Sobaszek, R. Bogdanowicz, K. Darowicki, J. Ryl,  
665 Multifrequency nanoscale impedance microscopy (m-NIM): A novel approach towards  
666 detection of selective and subtle modifications on the surface of polycrystalline boron-doped  
667 diamond electrodes, *Ultramicroscopy*. 199 (2019) 34–45.  
668 <https://doi.org/10.1016/j.ultramic.2019.01.004>.
- 669 [32] A. Mezni, M.M. Ibrahim, M. El-Kemary, A.A. Shaltout, N.Y. Mostafa, J. Ryl, T.  
670 Kumeria, T. Altalhi, M.A. Amin, Cathodically activated Au/TiO<sub>2</sub> nanocomposite synthesized  
671 by a new facile solvothermal method: An efficient electrocatalyst with Pt-like activity for  
672 hydrogen generation, *Electrochimica Acta*. 290 (2018) 404–418.  
673 <https://doi.org/10.1016/j.electacta.2018.08.083>.
- 674 [33] J. Kloubek, Development of methods for surface free energy determination using  
675 contact angles of liquids on solids, *Advances in Colloid and Interface Science*. 38 (1992) 99–  
676 142. [https://doi.org/10.1016/0001-8686\(92\)80044-X](https://doi.org/10.1016/0001-8686(92)80044-X).
- 677 [34] C.J. van Oss, Acid–base interfacial interactions in aqueous media, *Colloids and*  
678 *Surfaces A: Physicochemical and Engineering Aspects*. 78 (1993) 1–49.  
679 [https://doi.org/10.1016/0927-7757\(93\)80308-2](https://doi.org/10.1016/0927-7757(93)80308-2).
- 680 [35] D.K. Owens, R.C. Wendt, Estimation of the surface free energy of polymers, *Journal*  
681 *of Applied Polymer Science*. 13 (1969) 1741–1747.  
682 <https://doi.org/10.1002/app.1969.070130815>.
- 683 [36] T. Swebosci, P. Niedziałkowski, A. Cirocka, E. Szczepańska, T. Ossowski, A. Weisło,  
684 In pursuit of key features for constructing electrochemical biosensors – electrochemical and  
685 acid-base characteristic of self-assembled monolayers on gold, *Supramolecular Chemistry*. 0  
686 (2020) 1–11. <https://doi.org/10.1080/10610278.2020.1739685>.
- 687 [37] S. Shahrokhian, A. Mahdavi-Shakib, M. Ghalkhani, R. Saberi, Gold Electrode  
688 Modified with Self-Assembled Monolayer of Cysteamine-Functionalized MWCNT and Its  
689 Application in Simultaneous Determination of Dopamine and Uric Acid, *Electroanalysis*. 24  
690 (2012) 425–432. <https://doi.org/10.1002/elan.201100545>.
- 691 [38] C. Poitras, N. Tufenkji, A QCM-D-based biosensor for E. coli O157:H7 highlighting

692 the relevance of the dissipation slope as a transduction signal, *Biosensors and Bioelectronics*.  
693 24 (2009) 2137–2142. <https://doi.org/10.1016/j.bios.2008.11.016>.

694 [39] Y. Zhang, Y. Li, W. Wu, Y. Jiang, B. Hu, Chitosan coated on the layers' glucose  
695 oxidase immobilized on cysteamine/Au electrode for use as glucose biosensor, *Biosensors*  
696 and *Bioelectronics*. 60 (2014) 271–276. <https://doi.org/10.1016/j.bios.2014.04.035>.

697 [40] R.K. Shervedani, S.A. Mozaffari, Copper(II) Nanosensor Based on a Gold Cysteamine  
698 Self-Assembled Monolayer Functionalized with Salicylaldehyde, *Anal. Chem.* 78 (2006)  
699 4957–4963. <https://doi.org/10.1021/ac052292y>.

700 [41] R.K. Shervedani, M. Bagherzadeh, S.A. Mozaffari, Determination of dopamine in the  
701 presence of high concentration of ascorbic acid by using gold cysteamine self-assembled  
702 monolayers as a nanosensor, *Sensors and Actuators B: Chemical*. 115 (2006) 614–621.  
703 <https://doi.org/10.1016/j.snb.2005.10.027>.

704 [42] W.X. Cheng, D.Y. Peng, C.H. Lu, C.W. Fang, Direct electrochemical behavior of the  
705 Cysteamine/DNA/SWNTs-film-modified Au electrode and its interaction with taxol, *Russ J*  
706 *Electrochem.* 44 (2008) 1052–1057. <https://doi.org/10.1134/S1023193508090103>.

707 [43] K. De Wael, H. Buschop, L. De Smet, A. Adriaens, Immobilization of cytochrome c  
708 on cysteamine-modified gold electrodes with EDC as coupling agent, *Talanta*. 76 (2008) 309–  
709 313. <https://doi.org/10.1016/j.talanta.2008.02.040>.

710 [44] G.-Z. Garyfallou, O. Ketebu, S. Şahin, E.B. Mukaetova-Ladinska, M. Catt, E.H. Yu,  
711 Electrochemical Detection of Plasma Immunoglobulin as a Biomarker for Alzheimer's  
712 Disease, *Sensors*. 17 (2017) 2464. <https://doi.org/10.3390/s17112464>.

713 [45] M.M.S. Silva, I.T. Cavalcanti, M.F. Barroso, M.G.F. Sales, R.F. Dutra, Gold electrode  
714 modified by self-assembled monolayers of thiols to determine DNA sequences hybridization,  
715 *J Chem Sci.* 122 (2010) 911–917. <https://doi.org/10.1007/s12039-010-0079-7>.

716 [46] M. Wirde, U. Gelius, L. Nyholm, Self-Assembled Monolayers of Cystamine and  
717 Cysteamine on Gold Studied by XPS and Voltammetry, *Langmuir*. 15 (1999) 6370–6378.  
718 <https://doi.org/10.1021/la9903245>.

719 [47] K. Malecka, L. Michalczyk, H. Radecka, J. Radecki, Ion-Channel Genosensor for the  
720 Detection of Specific DNA Sequences Derived from Plum Pox Virus in Plant Extracts,  
721 *Sensors*. 14 (2014) 18611–18624. <https://doi.org/10.3390/s141018611>.

722 [48] G. Ilangovan, K. Chandrasekara Pillai, Electrochemical and XPS Characterization of  
723 Glassy Carbon Electrode Surface Effects on the Preparation of a Monomeric Molybdate(VI)-  
724 Modified Electrode, *Langmuir*. 13 (1997) 566–575. <https://doi.org/10.1021/la960053n>.

725 [49] J. Ryl, L. Burczyk, R. Bogdanowicz, M. Sobaszek, K. Darowicki, Study on surface  
726 termination of boron-doped diamond electrodes under anodic polarization in H<sub>2</sub>SO<sub>4</sub> by  
727 means of dynamic impedance technique, *Carbon*. 96 (2016) 1093–1105.  
728 <https://doi.org/10.1016/j.carbon.2015.10.064>.

729 [50] M. Sobaszek, K. Siuzdak, J. Ryl, M. Sawczak, S. Gupta, S.B. Carrizosa, M. Ficek, B.  
730 Dec, K. Darowicki, R. Bogdanowicz, Diamond Phase (sp<sup>3</sup>-C) Rich Boron-Doped Carbon  
731 Nanowalls (sp<sup>2</sup>-C): Physicochemical and Electrochemical Properties, *J. Phys. Chem. C*. 121  
732 (2017) 20821–20833. <https://doi.org/10.1021/acs.jpcc.7b06365>.

733 [51] M. Ficek, K.J. Sankaran, J. Ryl, R. Bogdanowicz, I.-N. Lin, K. Haenen, K. Darowicki,  
734 Ellipsometric investigation of nitrogen doped diamond thin films grown in microwave  
735 CH<sub>4</sub>/H<sub>2</sub>/N<sub>2</sub> plasma enhanced chemical vapor deposition, *Appl. Phys. Lett.* 108 (2016)  
736 241906. <https://doi.org/10.1063/1.4953779>.

737 [52] J. Wysocka, M. Cieslik, S. Krakowiak, J. Ryl, Carboxylic acids as efficient corrosion  
738 inhibitors of aluminium alloys in alkaline media, *Electrochimica Acta*. 289 (2018) 175–192.  
739 <https://doi.org/10.1016/j.electacta.2018.08.070>.

740 [53] J. Wysocka, S. Krakowiak, J. Ryl, Evaluation of citric acid corrosion inhibition  
741 efficiency and passivation kinetics for aluminium alloys in alkaline media by means of



- 742 dynamic impedance monitoring, *Electrochimica Acta*. 258 (2017) 1463–1475.  
743 <https://doi.org/10.1016/j.electacta.2017.12.017>.
- 744 [54] Q. Liu, X. Tong, G. Zhou, H<sub>2</sub>O Dissociation-Induced Aluminum Oxide Growth on  
745 Oxidized Al(111) Surfaces, *Langmuir*. 31 (2015) 13117–13126.  
746 <https://doi.org/10.1021/acs.langmuir.5b02769>.
- 747 [55] P. Niedziałkowski, R. Bogdanowicz, P. Zięba, J. Wysocka, J. Ryl, M. Sobaszek, T.  
748 Ossowski, Melamine-modified Boron-doped Diamond towards Enhanced Detection of  
749 Adenine, Guanine and Caffeine, *Electroanalysis*. 28 (2016) 211–221.  
750 <https://doi.org/10.1002/elan.201500528>.
- 751 [56] P. Niedziałkowski, T. Ossowski, P. Zięba, A. Cirocka, P. Rochowski, S.J. Pogorzelski,  
752 J. Ryl, M. Sobaszek, R. Bogdanowicz, Poly-l-lysine-modified boron-doped diamond  
753 electrodes for the amperometric detection of nucleic acid bases, *Journal of Electroanalytical*  
754 *Chemistry*. 756 (2015) 84–93. <https://doi.org/10.1016/j.jelechem.2015.08.006>.
- 755 [57] J.-B. Jorcin, M.E. Orazem, N. Pébère, B. Tribollet, CPE analysis by local  
756 electrochemical impedance spectroscopy, *Electrochimica Acta*. 51 (2006) 1473–1479.  
757 <https://doi.org/10.1016/j.electacta.2005.02.128>.
- 758 [58] P. Zoltowski, On the electrical capacitance of interfaces exhibiting constant phase  
759 element behaviour, *Journal of Electroanalytical Chemistry*. 443 (1998) 149–154.  
760 [https://doi.org/10.1016/S0022-0728\(97\)00490-7](https://doi.org/10.1016/S0022-0728(97)00490-7).
- 761 [59] P. Córdoba-Torres, T.J. Mesquita, O. Devos, B. Tribollet, V. Roche, R.P. Nogueira,  
762 On the intrinsic coupling between constant-phase element parameters  $\alpha$  and  $Q$  in  
763 electrochemical impedance spectroscopy, *Electrochimica Acta*. 72 (2012) 172–178.  
764 <https://doi.org/10.1016/j.electacta.2012.04.020>.
- 765 [60] R.K. Shervedani, S.A. Mozaffari, Impedimetric sensing of uranyl ion based on  
766 phosphate functionalized cysteamine self-assembled monolayers, *Analytica Chimica Acta*.  
767 562 (2006) 223–228. <https://doi.org/10.1016/j.aca.2006.01.046>.
- 768 [61] J. Wysocka, M. Cieslik, S. Krakowiak, J. Ryl, Carboxylic acids as efficient corrosion  
769 inhibitors of aluminium alloys in alkaline media, *Electrochimica Acta*. 289 (2018) 175–192.  
770 <https://doi.org/10.1016/j.electacta.2018.08.070>.
- 771 [62] P. Niedziałkowski, P. Slepski, J. Wysocka, J. Chamier-Cieminska, L. Burczyk, M.  
772 Sobaszek, A. Wcisło, T. Ossowski, R. Bogdanowicz, J. Ryl, Multisine impedimetric probing  
773 of biocatalytic reactions for label-free detection of DEF $\beta$ 1 gene: How to verify that your dog  
774 is not human?, *Sensors and Actuators B: Chemical*. 323 (2020) 128664.  
775 <https://doi.org/10.1016/j.snb.2020.128664>.
- 776 [63] R.K. Shervedani, S.A. Mozaffari, Impedimetric sensing of uranyl ion based on  
777 phosphate functionalized cysteamine self-assembled monolayers, *Analytica Chimica Acta*.  
778 562 (2006) 223–228. <https://doi.org/10.1016/j.aca.2006.01.046>.
- 779 [64] N. Borghol, L. Mora, T. Jouenne, N. Jaffézic-Renault, N. Sakly, A.C. Duncan, Y.  
780 Chevalier, P. Lejeune, A. Othmane, Monitoring of *E. coli* immobilization on modified gold  
781 electrode: A new bacteria-based glucose sensor, *Biotechnol Bioproc E*. 15 (2010) 220–228.  
782 <https://doi.org/10.1007/s12257-009-0146-4>.
- 783 [65] C. Tlili, E. Sokullu, M. Safavieh, M. Tolba, M.U. Ahmed, M. Zourob, Bacteria  
784 Screening, Viability, And Confirmation Assays Using Bacteriophage-Impedimetric/Loop-  
785 Mediated Isothermal Amplification Dual-Response Biosensors, *Anal. Chem*. 85 (2013) 4893–  
786 4901. <https://doi.org/10.1021/ac302699x>.
- 787 [66] P. Hashemi, A. Afkhami, H. Bagheri, S. Amidi, T. Madrakian, Fabrication of a novel  
788 impedimetric sensor based on l-Cysteine/Cu(II) modified gold electrode for sensitive  
789 determination of ampyra, *Analytica Chimica Acta*. 984 (2017) 185–192.  
790 <https://doi.org/10.1016/j.aca.2017.06.038>.
- 791 [67] R.K. Shervedani, A. Farahbakhsh, M. Bagherzadeh, Functionalization of gold

792 cysteamine self-assembled monolayer with ethylenediaminetetraacetic acid as a novel  
793 nanosensor, *Analytica Chimica Acta*. 587 (2007) 254–262.  
794 <https://doi.org/10.1016/j.aca.2007.01.053>.  
795 [68] R.K. Shervedani, M. Bagherzadeh, S.A. Mozaffari, Determination of dopamine in the  
796 presence of high concentration of ascorbic acid by using gold cysteamine self-assembled  
797 monolayers as a nanosensor, *Sensors and Actuators B: Chemical*. 115 (2006) 614–621.  
798 <https://doi.org/10.1016/j.snb.2005.10.027>.  
799 [69] R.K. Shervedani, S.A. Mozaffari, Copper(II) Nanosensor Based on a Gold Cysteamine  
800 Self-Assembled Monolayer Functionalized with Salicylaldehyde, *Anal. Chem.* 78 (2006)  
801 4957–4963. <https://doi.org/10.1021/ac052292y>.  
802 [70] Z. Li, L. Zhang, H. Mo, Y. Peng, H. Zhang, Z. Xu, C. Zheng, Z. Lu, Size-fitting effect  
803 for hybridization of DNA/mercaptohexanol mixed monolayers on gold, *Analyst*. 139 (2014)  
804 3137–3145. <https://doi.org/10.1039/C4AN00280F>.  
805 [71] M. Tolba, M.U. Ahmed, C. Tlili, F. Eichenseher, M.J. Loessner, M. Zourob, A  
806 bacteriophage endolysin-based electrochemical impedance biosensor for the rapid detection of  
807 *Listeria* cells, *Analyst*. 137 (2012) 5749–5756. <https://doi.org/10.1039/C2AN35988J>.  
808 [72] H. Xiang, Y. Wang, M. Wang, Y. Shao, Y. Jiao, Y. Zhu, A redox cycling-amplified  
809 electrochemical immunosensor for  $\alpha$ -fetoprotein sensitive detection via polydopamine  
810 nanolabels, *Nanoscale*. 10 (2018) 13572–13580. <https://doi.org/10.1039/C8NR02946F>.  
811 [73] K. Siuzdak, P. Niedziałkowski, M. Sobaszek, T. Łęga, M. Sawczak, E. Czaczyk, K.  
812 Dziąbowska, T. Ossowski, D. Nidzworski, R. Bogdanowicz, Biomolecular influenza virus  
813 detection based on the electrochemical impedance spectroscopy using the nanocrystalline  
814 boron-doped diamond electrodes with covalently bound antibodies, *Sensors and Actuators B:*  
815 *Chemical*. 280 (2019) 263–271. <https://doi.org/10.1016/j.snb.2018.10.005>.  
816 [74] D. Nidzworski, K. Siuzdak, P. Niedziałkowski, R. Bogdanowicz, M. Sobaszek, J. Ryl,  
817 P. Weiher, M. Sawczak, E. Wnuk, W.A. Goddard, A. Jaramillo-Botero, T. Ossowski, A rapid-  
818 response ultrasensitive biosensor for influenza virus detection using antibody modified boron-  
819 doped diamond, *Scientific Reports*. 7 (2017) 15707. [https://doi.org/10.1038/s41598-017-](https://doi.org/10.1038/s41598-017-15806-7)  
820 [15806-7](https://doi.org/10.1038/s41598-017-15806-7).  
821 [75] K.M. Zak, P. Grudnik, K. Guzik, B.J. Zieba, B. Musielak, A. Dömling, G. Dubin, T.A.  
822 Holak, Structural basis for small molecule targeting of the programmed death ligand 1 (PD-  
823 L1), *Oncotarget*. 7 (2016) 30323–30335. <https://doi.org/10.18632/oncotarget.8730>.  
824 [76] K.M. Zak, P. Grudnik, K. Magiera, A. Dömling, G. Dubin, T.A. Holak, Structural  
825 Biology of the Immune Checkpoint Receptor PD-1 and Its Ligands PD-L1/PD-L2, *Structure*.  
826 25 (2017) 1163–1174. <https://doi.org/10.1016/j.str.2017.06.011>.  
827 [77] D. Shi, X. An, Q. Bai, Z. Bing, S. Zhou, H. Liu, X. Yao, Computational Insight Into  
828 the Small Molecule Intervening PD-L1 Dimerization and the Potential Structure-Activity  
829 Relationship, *Front. Chem.* 7 (2019). <https://doi.org/10.3389/fchem.2019.00764>.  
830 [78] W. Liu, S.C. Garrett, E.V. Fedorov, U.A. Ramagopal, S.J. Garforth, J.B. Bonanno,  
831 S.C. Almo, Structural Basis of CD160:HVEM Recognition, *Structure*. (2019).  
832 <https://doi.org/10.1016/j.str.2019.05.010>.  
833 [79] R.J. Greenwald, G.J. Freeman, A.H. Sharpe, The B7 Family Revisited, *Annual*  
834 *Review of Immunology*. 23 (2005) 515–548.  
835 <https://doi.org/10.1146/annurev.immunol.23.021704.115611>.  
836